Applications of the Multilayer Porous Medium Modeling Approach for Noise Mitigation

Teruna, Christopher; Rego, Leandro; Avallone, Francesco; Ragni, Daniele; Casalino, Damiano

DOI
10.1061/(ASCE)AS.1943-5525.0001326

Publication date
2021

Document Version
Final published version

Published in
Journal of Aerospace Engineering

Citation (APA)
Teruna, C., Rego, L., Avallone, F., Ragni, D., & Casalino, D. (2021). Applications of the Multilayer Porous Medium Modeling Approach for Noise Mitigation. *Journal of Aerospace Engineering*, *34*(6), Article 04021074. https://doi.org/10.1061/(ASCE)AS.1943-5525.0001326

ASCE

Applications of the Multilayer Porous Medium Modeling Approach for Noise Mitigation

Christopher Teruna[1]; Leandro Rego[2]; Francesco Avallone[3]; Daniele Ragni[4]; and Damiano Casalino[5]

Abstract: Porous materials have been widely investigated as a mean for noise reduction. Numerical simulations can be used to investigate the physical mechanisms responsible for noise reduction; however, a correct modeling of the porous medium through an equivalent fluid model is essential to minimize the computational costs. This paper reports a detailed review of a few applications of the equivalent fluid model based on a three-layer approach, a method that is particularly useful to account for the variation of porous material thickness in aerospace applications. The multilayer approach has been applied in three relevant aerodynamic noise issues: leading-edge impingement noise, turbulent boundary-layer trailing-edge noise, and jet installation noise. Comparison with experiments is used to validate the simulation approach. **DOI: 10.1061/(ASCE)AS.1943-5525.0001326.**

Author keywords: Aerodynamic noise; Porous material; Noise reduction; Numerical simulations; Multilayer model.

Introduction

Aerodynamic noise is often the side product of the interaction between turbulence and solid bodies. For example, when an airfoil is immersed in a turbulent flow field, the turbulence-impingement process at the leading edge (LE) would result in noise radiation. This mechanism is commonly found in rotorcrafts (blade-vortex interaction) (Lee and Smith 1991; Wie et al. 2011) as well as in high-bypass turbofans (fan wake-outlet guide vane interaction) (Casalino et al. 2018). In the absence of turbulent inflow, turbulence can also be generated inside the boundary layer on an airfoil at high Reynolds numbers, and when it interacts with the trailing edge, noise is also scattered. Such turbulent boundary-layer trailing-edge (TBL-TE) noise is one of the main noise-generation mechanisms for wind turbine blades (Oerlemans et al. 2009) and high-lift devices (Brooks and Humphreys 2003). Analogously, high-lift devices also behave as strong noise radiators when interacting with the near field of jet engine exhaust (Self 2004), which is referred to as jet installation noise (JIN) (Lawrence et al. 2011).

As regulations surrounding aviation and wind turbine noise become stricter, it is of paramount interest for the industry to develop noise-mitigation solutions. In general, LE and TE noise generation can be considered as an acoustic scattering problem due to turbulent structures encountering a sudden change in surface boundary condition (Amiet 1975, 1976; Howe 1978). It was suggested that a permeable edge could promote a less abrupt transition instead (Herr and Dobrzynski 2005). Despite this, LE and TE noise mechanisms are different in nature; thus, applying permeable treatments can be expected to produce different noise-mitigation mechanisms. For instance, porous LE application allows for suppressing sound source intensity by reducing the amplitude of surface pressure fluctuations during turbulence-impingement events (Lee and Smith 1991). Differently, a porous TE reduces the scattering efficiency of the TE (Cavalieri et al. 2016) and introduces multiple scattering events such that destructive interference would occur (Kisil and Ayton 2018). The application of permeable materials have also shown promising capability in different situations, such as for addressing LE noise (Roger et al. 2013; Zamponi et al. 2020), TBL-TE noise (Geyer and Sarradj 2014; Rubio Carpio et al. 2017; Teruna et al. 2020), and JIN (Rego et al. 2021).

One of the earliest practical application of permeable treatment was to mitigate jet-flap interaction noise (Hayden 1973), where it was found that applying porosity could produce up to 10 dB of noise reduction. Permeable blades were also used in an attempt to reduce fan noise emissions (Chanaud et al. 1976). It has been considered that the properties of the porous materials could be tuned to reach the highest noise-reduction potential. For this purpose, different types of porous materials have been investigated, ranging from perforated structures (Jiang et al. 2018; Rubio Carpio et al. 2020) to more complex geometries such as granulates and metal foams (Roger et al. 2013; Geyer and Sarradj 2019; Rubio Carpio et al. 2017).

It has been shown that the properties of these materials are strongly related to the noise-reduction level. In general, porous materials with very high porosity and permeability tend to produce higher noise-reduction levels (Rubio Carpio et al. 2017), although this was often accompanied by high-frequency excess noise (Herr et al. 2014). Increasing the porous edge extent is also found to improve noise attenuation, but this may lead to severe aerodynamic performance impact (Geyer and Sarradj 2014). Considering the

[1]Ph.D. Candidate, Faculty of Aerospace Engineering, Delft Univ. of Technology, Kluyverweg 1, 2629 HS Delft, Netherlands (corresponding author). ORCID: https://orcid.org/0000-0003-4755-9592. Email: c.teruna@tudelft.nl

[2]Ph.D. Candidate, Faculty of Aerospace Engineering, Delft Univ. of Technology, Kluyverweg 1, 2629 HS Delft, Netherlands. Email: l.rego@tudelft.nl

[3]Assistant Professor, Faculty of Aerospace Engineering, Delft Univ. of Technology, Kluyverweg 1, 2629 HS Delft, Netherlands. ORCID: https://orcid.org/0000-0002-6214-5200. Email: f.avallone@tudelft.nl

[4]Associate Professor, Faculty of Aerospace Engineering, Delft Univ. of Technology, Kluyverweg 1, 2629 HS Delft, Netherlands. Email: d.ragni@tudelft.nl

[5]Professor, Faculty of Aerospace Engineering, Delft Univ. of Technology, Kluyverweg 1, 2629 HS Delft, Netherlands. Email: d.casalino@tudelft.nl

Note. This manuscript was submitted on November 24, 2020; approved on May 12, 2021; published online on July 24, 2021. Discussion period open until December 24, 2021; separate discussions must be submitted for individual papers. This paper is part of the ***Journal of Aerospace Engineering***, © ASCE, ISSN 0893-1321.

presence of such trade-offs, a good understanding of the noise-reduction mechanisms is necessary in order to better optimize the different porous material applications.

The working principles of permeable-edge treatment have been studied using analytical approaches (Cavalieri et al. 2016; Kisil and Ayton 2018), but these approaches tend to be limited to simplified configurations, such as a perforate flat plate. More realistic configurations can be addressed using experiments, but to perform measurements inside and around a permeable LE/TE could be quite challenging (Ali et al. 2018). As an alternative, high-fidelity numerical simulations may offer higher data density and spatial resolution compared with experiments. However, it might be impractical to consider the geometrical details of the porous medium, including those that are smaller than turbulent scales expected in the inertial subrange, because this could incur heavy computational costs. A modeling approach that represents the macroparameters of the material may serve as a viable alternative to reduce the computational effort and at the same time maintain high fidelity to reality.

Furthermore, it is essential to find a modeling strategy that can be used in several practical applications, where, for example, the material geometry may vary (i.e., a change of thickness at the leading edge or trailing edge). This paper explores several applications of the porous medium model in a lattice-Boltzmann solver. Firstly, a validation study is performed by replicating a porous material characterization test rig. Then, the porous medium model is employed for different aeroacoustic problems, such as LE, TBL-TE, and JIN reduction. Simulation results are validated against experimental data, and the benefits provided by the porous materials are assessed through comparison with the baseline configurations.

The rest of this paper is organized as follows. The numerical method, which is based on the Lattice-Boltzmann method coupled with a very large eddy simulation (LBM-VLES) implemented in the commercial software SIMULIA PowerFLOW version 5.4b, is reported in the next section. Then, the subsequent section discusses the procedure of porous material characterization and the numerical modeling approach. Several examples showing the applications of the porous medium model are provided afterward, followed by a brief summary of present findings.

Flow Solver

The flow field has been computed using the commercial software SIMULIA PowerFLOW 6-2019, which is based on LBM-VLES. This method solves the discrete form of the Boltzmann equation by explicitly tracking the development of particle distribution functions at the mesoscopic scale. The Navier-Stokes equations can be recovered through the Chapman-Enskog expansion, and fluid properties such as density, momentum, and internal energy are obtained through a local integration of the particle distribution (Succi 2001). The solution of the Boltzmann equation is performed on a Cartesian mesh (lattice), with an explicit time integration and collision model.

A VLES model accounts for the unresolved scales of turbulence. A modified two-equations $k-\epsilon$ renormalization group (RNG) turbulence model is employed to compute a turbulent relaxation time that is added to the viscous relaxation time (Yakhot and Orszag 1986). The relaxation time is then used to adapt the Boltzmann model to the characteristic time scales of a turbulent flow motion. Hence, the Reynolds stresses are not explicitly derived from to the governing equations, but they are an implicit consequence of the chaotic exchange of momentum driven by the turbulent flow, with characteristic times smaller than the slowly varying turbulent flow. The Reynolds stresses then have a nonlinear structure and are better suited to represent turbulence in a state far from equilibrium, as in the presence of distortion, shear, and rotation (Chen et al. 2004). A wall model is also adopted to approximate the no-slip boundary conditions, which is based on an extension of the generalized law-of-the-wall model, taking into account the effect of pressure gradients (Launder and Spalding 1974).

For the applications in this paper, the far-field noise is computed through the Ffowcs-Williams and Hawkings (FW-H) analogy (Ffowcs-Williams and Hawkings 1969), adopting Formulation 1A from Farassat extended to a convective wave equation (Brès et al. 2010; Farassat and Succi 1980). The formulation is implemented in the time domain using a source-time-dominant algorithm (Casalino 2003).

Numerical Modeling of Porous Medium

Characterization of Porous Medium

In general, porous media refer to solid materials with embedded voids (Morreale and Shi 2015). These materials generally have relatively low density compared with that of fully solid materials with large area-to-volume ratio. Porous media fall in the category of metamaterials, engineered to promote specific properties depending on their applications, which may otherwise not be found in nature (Kshetrimayum 2004). Based on the flow-transport properties, porous media can be characterized by up to six different parameters (Ingham and Pop 1998), although the most common ones are porosity, permeability (viscous resistivity), and form coefficient (inertial resistivity) (Sarradj and Geyer 2007; Liu et al. 2015; Rubio Carpio et al. 2017). The porosity of a porous medium ϕ is defined as follows:

$$\phi = 1 - \frac{\rho_p}{\rho_m} \tag{1}$$

where ρ_p and ρ_m = density of the porous medium and that of the matrix, respectively. The porous medium density can be obtained by measuring the weight of the porous medium sample for a given volume (Rubio Carpio et al. 2017). Other methods for obtaining porosity can be found in the literature (Rouquerol et al. 1994).

Permeability K and form coefficient C are parameters that determine the amount of resistance encountered by the flow permeating through the porous medium. These parameters also appear in the Hazen-Dupuit-Darcy equation (Ingham and Pop 1998), which describes the pressure loss Δp across a porous medium sample of thickness t as follows:

$$\frac{\Delta p}{t} = \frac{\mu_\infty}{K} v_d + \rho_\infty C v_d^2$$
$$\frac{\Delta p}{\rho_\infty t} = R_V v_d + R_I v_d^2 \tag{2}$$

where μ_∞ and ρ_∞ = fluid's dynamic viscosity and density, respectively; and v_d = Darcian velocity, i.e., average flow velocity inside the porous material.

It can be observed that the equation is a second-order polynomial with respect to the Darcian velocity. The linear term of the equation refers to the contribution of viscous effects inside the porous material, and thus the coefficient $\mu_\infty/(\rho_\infty K)$ is also referred to as the viscous resistivity R_V. The quadratic term describes the form drag (inertial forces) contribution of the porous material matrix, and thus the form coefficient C is also referred to as the inertial resistivity R_I. It is implied that as the velocity inside the porous medium becomes higher, the inertial resistance becomes more significant compared with the viscous one (Ingham and Pop 1998).

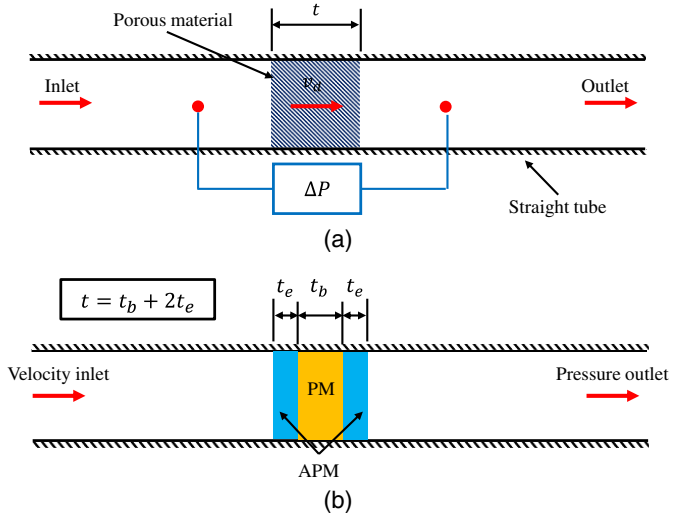

Fig. 1. (a) Porous material permeability test rig; and (b) its representation in the numerical simulation.

Following the Hazen-Dupuit-Darcy equation, it is clear that permeability and form coefficient can be obtained through curve-fitting of the pressure drop at different Darcian velocities. One such experiment has been performed in the past (Rubio Carpio et al. 2017) using a test rig as shown in Fig. 1(a). The test rig consists of a long straight tube, where a mass-flow regulator is installed at the inlet to control flow velocity inside the tube, and the outlet is exposed to the ambient atmosphere. The cylindrical porous medium sample is inserted at the middle of the tube. There are also two pressure taps located upstream and downstream of the porous medium from which the pressure drop value is measured. Rubio Carpio et al. (2017, 2018) have given further information on the experimental features and uncertainties.

It was found that the pressure drop curves tend to collapse on top of each other as the porous medium thickness was increased. This implies that the permeability and form coefficient of the porous medium also vary with sample thickness, at least before a critical thickness is reached. The same phenomenon has been observed in another investigation on the transport characteristics of metal foam (Baril et al. 2008). It was also reported that the critical thickness of the metal foam samples is about 40–50 times the mean pore diameter.

Baril et al. (2008) argued that the resistivity of a porous material is influenced by two different aspects: the entrance effect and the bulk effect. The entrance effect is related to the flow unsteadiness that occurs near the surface of the porous medium, in a region defined as the entrance length. The bulk effect dominates beyond the entrance length, where the flow field has become more steady after adapting to the environment inside the porous medium. Following this, it can be reasoned that the resistivity due to the bulk effect does not vary with the material thickness, unlike that caused by the entrance effect.

Numerical Modeling of Porous Medium

For investigating the different aeroacoustic applications of porous media, numerical simulations often provide more flexibility in data collection in comparison with experimental techniques (Teruna et al. 2020). In general, there are three main approaches for implementing porous media in simulations: (1) fully resolving the porous medium structure (Kuwata and Suga 2017), (2) representing the macroscopic effect of the porous medium in an equivalent fluid region (Ananthan et al. 2020), and (3) replacing the porous medium with an equivalent surface-impedance condition (Li et al. 2011). The first approach could easily become very expensive for porous materials whose pores are much smaller than the characteristic length of the main body. On the other hand, the third approach is limited because it only considers the aerodynamic interaction between the flow and the porous medium at the surface, and as a result the flow behavior inside the porous medium is neglected (Delfs et al. 2014).

Following this, the second approach, also commonly referred to as the volume-averaging approach, offers a good balance between the level of accuracy of flow behavior in the porous medium as well as computational cost. The lattice-Boltzmann solver SIMULIA PowerFLOW implements a volume-averaging approach based on the Darcy's law, which is used in the following investigations. This subsection hence briefly discusses the implementation of the porous medium modeling; more details have been given in the literature (Freed 1998; Sun et al. 2015).

A porous medium can be considered as a fluid region that introduces additional momentum loss, governed by the Darcy's law. The momentum loss is caused by a Darcy's force that can be mathematically described as follows:

$$\nabla p = -\boldsymbol{R} \cdot \boldsymbol{u} \tag{3}$$

where ∇p = pressure gradient along the porous medium; $\boldsymbol{u}$ = local flow velocity; and $\boldsymbol{R}$ = total resistivity, which includes both contributions of viscous and inertial resistivity components ($\boldsymbol{R}_V$ and $\boldsymbol{R}_I$, respectively). $\boldsymbol{R}$ can be expanded as in Eq. (4)

$$\boldsymbol{R} = \boldsymbol{R}_V + \boldsymbol{R}_I \boldsymbol{u}; \qquad \boldsymbol{R}_V = \frac{\mu_\infty}{\rho_\infty \boldsymbol{K}}, \qquad \boldsymbol{R}_I = \boldsymbol{C} \tag{4}$$

Using the Chapman-Enskog expansion up to third-order truncation for perfect gas at low Mach number (Chen et al. 1992), it can be shown that the Navier-Stokes equation can be recovered from the discrete Boltzmann equation. The resulting Navier-Stokes equation including the Darcy's force terms is shown in Eq. (6). In comparison with the regular Navier-Stokes equation, the regular viscous term in Eq. (6) has been replaced by the Darcy's force terms. This is valid for the porous medium region, but outside of it, the Darcy's force term vanishes and is replaced with the regular viscous term

$$\frac{\partial \rho}{\partial t} + \nabla \cdot (\rho \boldsymbol{u}) = 0 \tag{5}$$

$$\frac{\partial \rho \boldsymbol{u}}{\partial t} + \nabla \cdot (\rho \boldsymbol{u}\boldsymbol{u}) = -\nabla p - \boldsymbol{R} \cdot \boldsymbol{u} \tag{6}$$

There are two different porous medium models in PowerFLOW: acoustic porous medium (APM) and porous medium (PM). Darcy's force term is implemented in both models. However the APM model has an additional feature where an interface between the regular fluid region and the porous media region is created as double-sided surfaces, similar to a sliding mesh mechanism (Sun et al. 2015). In addition, the mass-flux conservation at the interface is determined by the porosity of the porous medium as shown in the following:

$$|\rho u_n|_\infty = \phi |\rho u_n|_{\mathrm{PM}} \tag{7}$$

where ϕ = material porosity; and subscripts ∞ and PM = regular fluid region and porous media region, respectively.

Both APM and PM models require both viscous and inertial resistivity values to be known a priori. In many cases, these values are obtained empirically before being applied into the porous medium models (Sun et al. 2015). However, surface roughness effects are not taken into account because the porous medium is modeled as equivalent uniform and homogeneous fluid region. This aspect in

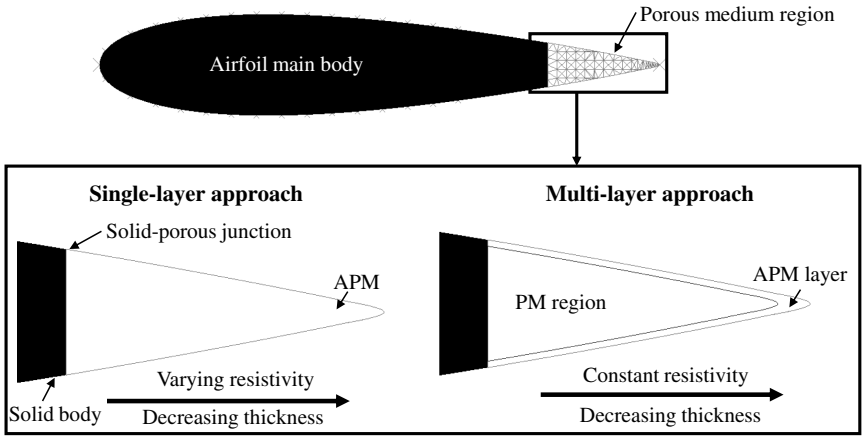

Fig. 2. Comparison between single-layer and multilayer approaches to porous medium modeling.

particular has been observed to have relevant contribution toward excess noise at high frequencies (Rubio Carpio et al. 2018; Geyer and Sarradj 2014) and in the disparity between experiments and simulations.

For aerodynamic bodies, it is often necessary to take into account the variation of permeability and form coefficient with the local thickness of the porous medium. Although this is not impossible to be ensured, it introduces additional level of complexity when preparing the simulations. To circumvent this issue, the authors have previously proposed the multilayer porous medium modeling approach (Teruna et al. 2020). The modeling technique involves isolating the entrance length of the porous medium as a separate region because the thickness-dependency of porous medium properties is due to the influence of the entrance effect. Such implementation is particularly useful, for instance, for airfoil with porous edges as shown in Fig. 2.

With a single-layer APM region, the local material resistivity varies from the solid-porous junction to the actual TE following the local thickness. With the multilayer approach, a separate APM layer of constant thickness is defined around the entrance length, and the rest of the porous medium is represented by the PM region. Hence, constant resistivity values corresponding to the APM layer thickness can be applied. The same applies for the PM region even though its thickness varies along the airfoil chord because it is dominated by the bulk resistivity that is independent of the material thickness.

Verification of the Multilayer Porous Medium Approach

To verify the multilayer approach, the porous material permeability test rig is simulated as shown in Fig. 1(b). The porous medium is inserted at the middle of a tube, consisting of three separate layers; the outer layer is modeled by APM and the inner one with PM. For the simulation, both APM layers account for 20% of the overall porous medium thickness, and the rest of the volume is prescribed as a PM region (i.e., $t_e = 0.1t$ and $t_b = 0.8t$). The thickness of the APM layer is specified to encompass the expected entrance length, and this criterion will be applied in the different applications shown subsequently. For this verification purpose, the APM layer thickness has been set to be proportional to the sample thickness to examine the sensitivity of the numerical solutions with the present approach.

The tube itself is 1.5 m long with a circular cross section of 55 mm in diameter. The pressure drop (Δp) is obtained by sampling pressure time history at locations 50-mm upstream and downstream of the porous medium. At the upstream end of the tube, a velocity inlet is prescribed, whereas at the other end, a static pressure outlet is applied. The porous material considered in the present applications is a metal-foam made of NiCrAl alloy manufactured by Alantum (Munich, Germany). Two types of metal foam are considered with different mean cell diameter d_c values of 450 and 800 μm, respectively.

To obtain the R_V and R_I values for the simulation, experiments are performed beforehand (Rubio Carpio et al. 2017), and the results are reported in Fig. 3(a). From the plot, it is clear that the metal foam with the smaller pore size imposes higher resistivity compared with the other. The inlet velocity is specified to be 2.35 and 2.55 m/s for 450- and 800-μm metal foam samples, respectively, as in the experiment. Subsequently, the resistivity values in Fig. 3(a) serve as the input for the simulation, and the resulting pressure drop values are shown in Fig. 3(b). The figure evidences that the simulations estimate well the pressure drop values.

Based on the results in this section, the porous medium models and the multilayer approach can be considered reliable for simulating flow-transport phenomena in a porous material. Nevertheless, the current applications are focused on the metal foam, which has isotropic and homogeneous resistivity. Hence, further investigations are warranted to determine the applicability of the present modeling approach for more specific types of porous materials.

Applications of Porous Medium Model for Aeroacoustics Problems

Turbulence Interaction Noise

In this application, simulations of a rod-airfoil configuration are carried out. This model was previously proposed as a simplified setup for replicating the effect of quasi-tonal excitation that is typically found in rotating machinery (Jacob et al. 2005). The simulation setup is shown in Fig. 4, depicting a rod placed upstream of a NACA 0012 airfoil. The airfoil has a chord length of $c = 100$ mm, which is also equal to the streamwise separation between the base of the rod to the airfoil leading edge; the rod diameter equals to $d = 0.1c = 10$ mm. Both the rod and airfoil have an identical span of 300 mm, and they are mounted on side plates which is installed at the outlet of a nozzle. The nozzle inlet condition is specified such that a mean outlet velocity of $U_\infty = 72$ m/s is achieved.

For noise prediction, a permeable FW-H surface has been prescribed to enclose the side plates and rod-airfoil setup, and consequently, installation effects are considered in the simulation. An acoustic sponge zone has been defined starting at a distance of $10c$ from the airfoil leading edge to prevent outward-traveling acoustic

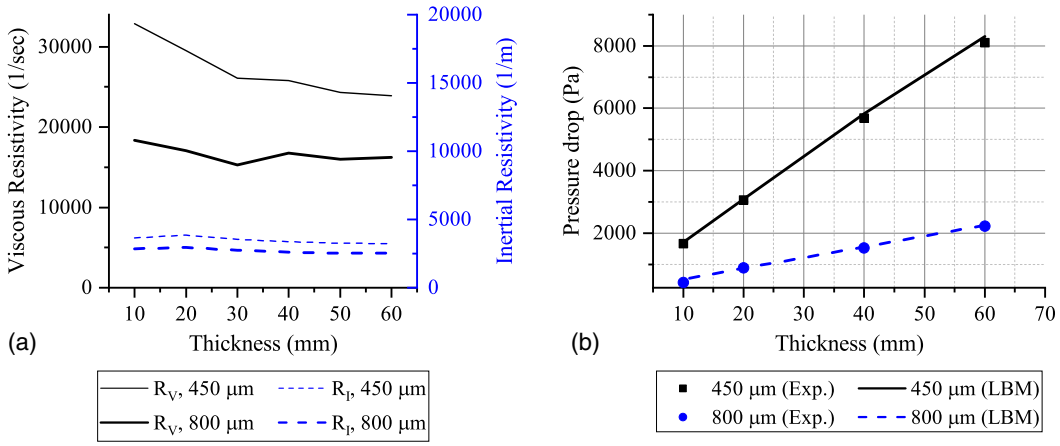

Fig. 3. (a) Resistivity values for the metal foam sample obtained from the experiment; and (b) comparison of the pressure drop result between the experiment (Exp.) and simulation (LBM).

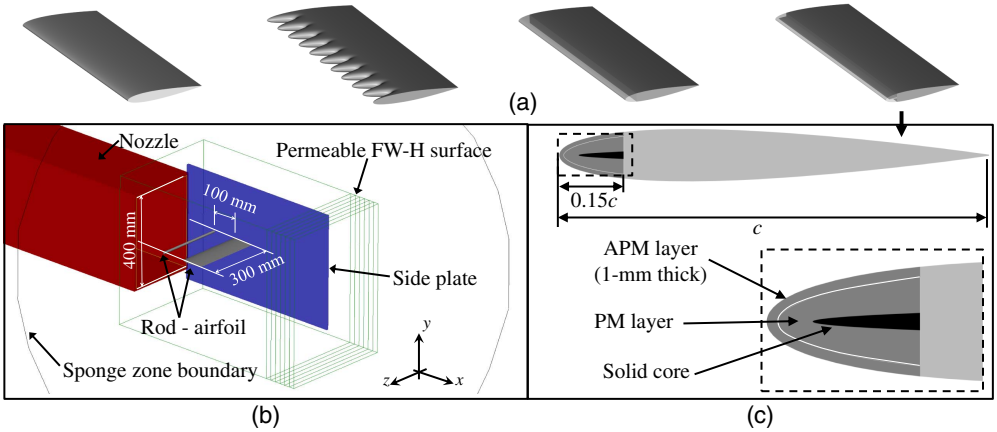

Fig. 4. (a) Leading-edge configurations that are considered in this study; (b) baseline setup of the rod-airfoil configuration, where the second side plate is hidden in this view; and (c) nomenclature and details of dimensions of the BLE.

waves from being reflected by the domain boundary back into the near-field region.

A total of four different LE treatments has been considered as shown in Fig. 4(a): the baseline solid LE (SLE), LE serrations (WLE), a regular porous LE (PLE), and a partially blocked porous LE (BLE). Although the serrations have a very different working principle than the porous LE (Narayanan et al. 2015), they are included as an example of state-of-the-art solution for LE noise mitigation. Both the serrations and porous treatments modify the first 15% of the airfoil chord. The LE serrations are designed with sinusoidal pattern with both the wavelength and the amplitude equal to $0.3c$ (Teruna et al. 2021), following the optimized parameters proposed in the literature (Narayanan et al. 2015).

The porous LE is modeled using the multilayer porous medium approach that was introduced in the previous section; a solid core is added along the chord line of the airfoil with BLE treatment. The latter is considered to investigate the effect of partially blocking the direct flow path between the suction and pressure sides of the airfoil. The porous material chosen for this application is the metal foam with mean pore size of 0.8 mm, and its properties (viscous and inertial resistivity) are shown in Fig. 3(a) and reported in Table 1. APM and PM layers have separate properties.

Table 1. Porosity (ϕ), viscous (R_V), and inertial (R_I) resistivity parameters applied to the equivalent fluid regions, which replicate the properties of a metal foam with cell diameter $d_c = 800$ μm

Region	ϕ (%)	R_V (s^{-1})	R_I (m^{-1})
APM	91.65	6,575	2,854
PM	—	5,489	2,520

The validation of far-field noise results are provided in Fig. 5, where the sound pressure spectra are plotted in Fig. 5(a) and far-field directivity pattern in Fig. 5(b). In Fig. 5(a), a microphone is placed at a distance of 1.85 m directly above the airfoil LE, i.e., at an observation angle of 90° with the 0° reference toward the downstream direction. Fig. 5(b) shows the overall sound pressure level (OSPL) along an arc on the x-y plane with a radius of 1.85 m. Both sound spectra and far-field directivity pattern from the simulation are in agreement with other reference data. There are notable discrepancies in between 40°–70° and 280°–310°, which are considered to be due to the slight difference in open jet shear-layer behavior between the simulation and the experiment because boundary-layer development along the nozzle wall is not replicated in the simulation. Nonetheless, this verifies that the current simulation setup is

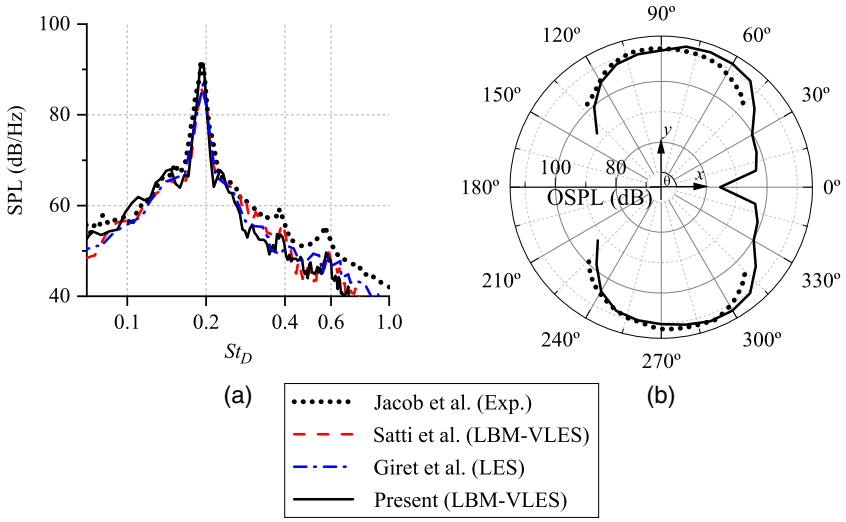

Fig. 5. (a) Far-field sound spectra; and (b) OSPL directivity pattern for the baseline (SLE) rod-airfoil configuration.

able to produce reliable aeroacoustics prediction for the rod-airfoil configuration.

The effects of the LE treatments on the far-field sound characteristics are illustrated in Fig. 6, where Fig. 6(a) shows the comparison of sound power level reduction, and Fig. 6(b) shows the directivity of OSPL. There are two frequency ranges presented in Fig. 6(a): the first one at $St_D = [0.15, 0.25]$ corresponds to the main tonal peak region; the second at $St_D = [0.25, 0.75]$ includes the broadband noise component. It is clear that the WLE configuration shows the highest noise attenuation with 4.5 and 8.9 dB for the broadband

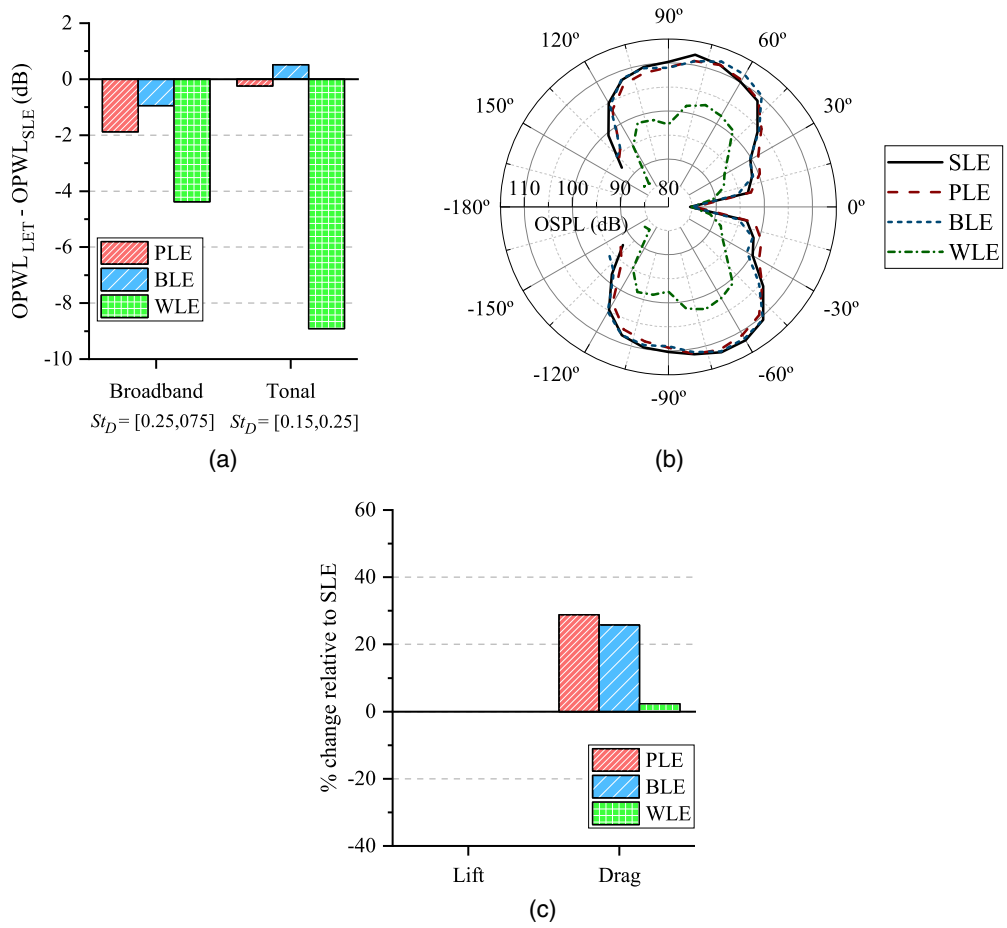

Fig. 6. (a) Overall sound power (OPWL) reduction level; (b) far-field directivity pattern; and (c) airfoil aerodynamic penalty of the rod-airfoil configuration equipped with different LE treatments.

and tonal noise component, respectively. Conversely, the PLE shows negligible attenuation of the tonal noise region, but the broadband one is reduced by 2 dB. The BLE exhibits the worst noise-reduction level out of the three LE treatments.

Based on Fig. 6(b), the LE treatments do not appear to alter noise directivity considering that the dipolelike pattern is still present in all cases. This implies the main noise-generation mechanism is identical for all cases, i.e., the lift fluctuations induced by turbulent eddies impinging the LE (Jacob et al. 2005). The aerodynamic impact of the different LE treatments is presented in Fig. 6(c). Because the airfoil is symmetric and also installed at a zero angle of attack, only the drag changes are relevant. The plot clearly shows that the porous LE incurs a significant drag increase (Teruna et al. 2020) by almost 50%. This can be associated with the rapid increase of the displacement thickness in the boundary layer downstream of the porous LE due to unsteady flow transpiration at the porous medium surface. On the other hand, the drag increase due to the LE serrations is relatively minor.

The present attempt of applying porous LE treatment is rather underwhelming, particularly in comparison with the LE serrations. However, this can be partly attributed to the fact that the metal foam material might not be the optimal choice for this purpose. Nevertheless, the results also suggest that it is necessary for the porous LE to be fully permeable in order to maximize noise-reduction level. Further investigations into the noise-mitigation mechanisms of porous LE applications are warranted, which could eventually lead to potential optimization techniques.

Turbulent Boundary-Layer Trailing-Edge Noise

A set of simulations have been carried out on a NACA 0018 airfoil equipped with a porous trailing-edge (TE) insert, as shown in Fig. 7. The simulation setup replicates that of a past experiment (Rubio Carpio et al. 2018). The airfoil has a chord length of $c = 200$ mm and a span of 80 mm; this span is only one-fifth of that in the experiment to reduce computational cost. The last 20% of the airfoil chord can be replaced with a porous insert that is based on a metal foam whose properties are reported in Table 1. The airfoil is installed at zero angle of attack and subject to a free-stream velocity of 20 m/s ($Re_c = 263{,}000$). Free-stream turbulence intensity is set to 0.1 % following the reference value from past experimental work (Merino-Martínez et al. 2020). An acoustic sponge region has been specified to mitigate unwanted sound reflection at the domain boundaries, starting from a radius of $36c$ away from the origin, which is located at the TE midspan (i.e., the airfoil LE is located at $x/c = -1$).

Two types of porous inserts are considered for this study, a fully permeable one (APM TE) and another with solid partition added along the chord line (NP TE). The NP TE is considered to study the effect of blocking direct flow path between the suction and pressure side of the airfoil. The internal arrangement of the porous medium model is also shown in Fig. 7 where an APM layer of a constant 1-mm thickness is applied on top of the PM layer; the solid partition is added inside the porous medium region for the NP TE configuration. Thus, the entrance length of the porous medium is fully contained within the APM layer. As indicated in the previous section, the multilayer modeling approach allows for applying constant resistivity values in either APM or PM layers in spite of the variation in local thickness of the porous insert. The voxel distribution surrounding the airfoil and the TE region is shown in Fig. 8.

Far-field noise is computed using the FW-H analogy based on surface pressure fluctuations, and the results are shown in Fig. 9. The observer is located directly above the TE location ($y/c = 5$). Fig. 9(a) compares the noise intensity produced by the different TE types. The APM TE is shown to produce substantial noise reduction (up to 10 dB), particularly at low frequencies. The noise-reduction level decreases gradually at the midfrequency range until it is nearly gone at higher frequencies. On the other hand, the NP TE shows very similar spectral characteristics as the solid (SLD) TE, and thus no noise reduction could be observed.

The same phenomena are illustrated in Fig. 9(b), where the noise-reduction level obtained from the simulation is compared with that from the experiment. Good agreement can be found at low-frequency to midfrequency range ($4 < St_c < 12$), and the slight discrepancy might have been caused by artefact in the porous medium model where the local APM layer thickness becomes smaller than the entrance length (e.g., near the last 1% of the airfoil chord). Nevertheless, the simulation results underpredict the high-frequency excess noise, which can be attributed to the fact that surface roughness effect has been neglected due to the porous medium model (Teruna et al. 2020). The present results clearly show that the noise-mitigation mechanism of the porous insert is linked to the flow interaction between both sides of the TE across the porous medium (Rubio Carpio et al. 2019).

The aerodynamic impact of the metal foam TE is relatively minor as shown in Fig. 10. The pressure distribution on the airfoil upstream of the solid-porous junction remains unaffected by the porous TE. A similar finding has been found in the experiment by Rubio Carpio et al. (2017). On the porous medium itself, the pressure coefficient is slightly lower than on the solid surface, which is attributed to the flow transpiration at the porous medium interface.

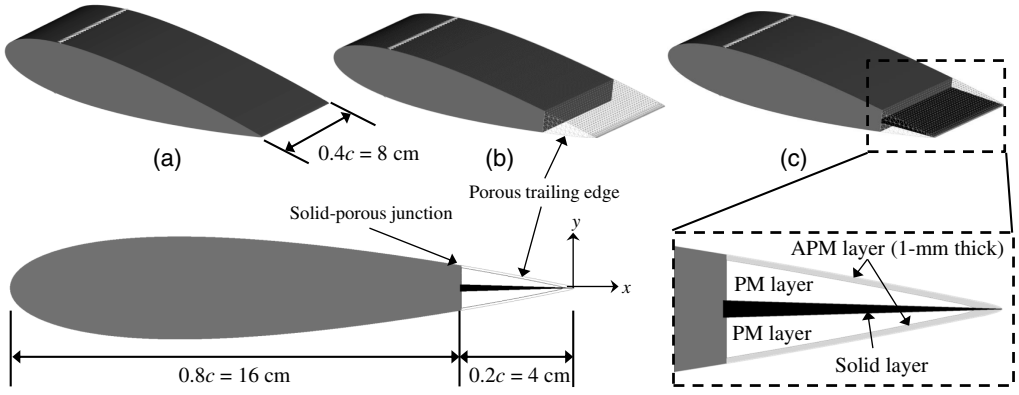

Fig. 7. NACA 0018 with three different TE configurations. A lateral view of the NP TE is also shown. An inset shows the internal arrangement of the NP TE.

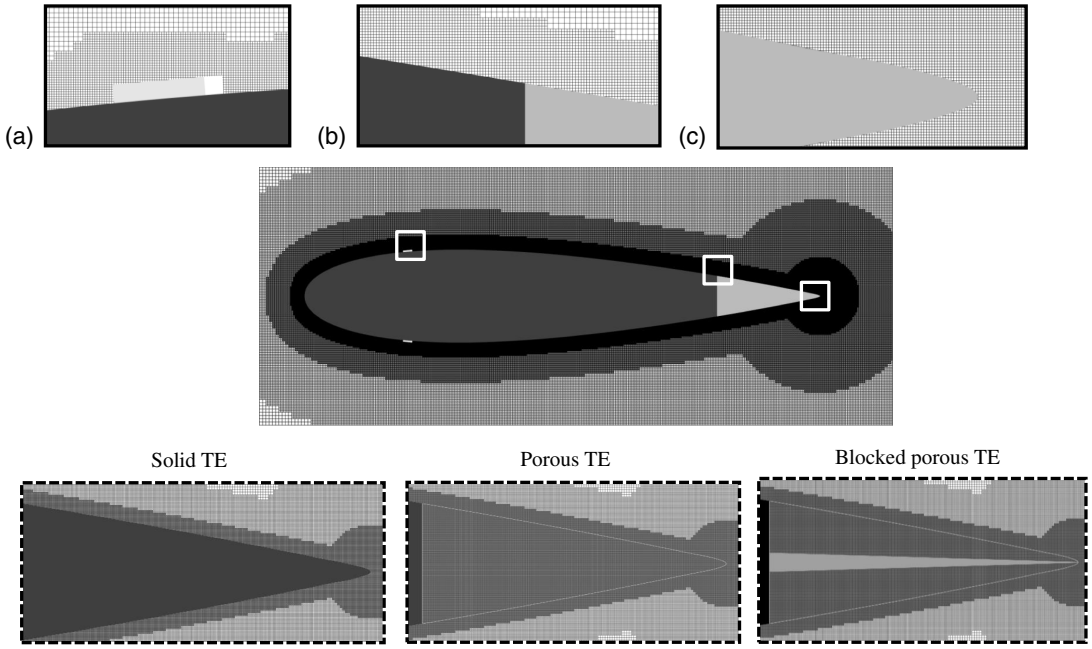

Fig. 8. Grid configuration for the NACA 0018 case with different TE configurations.

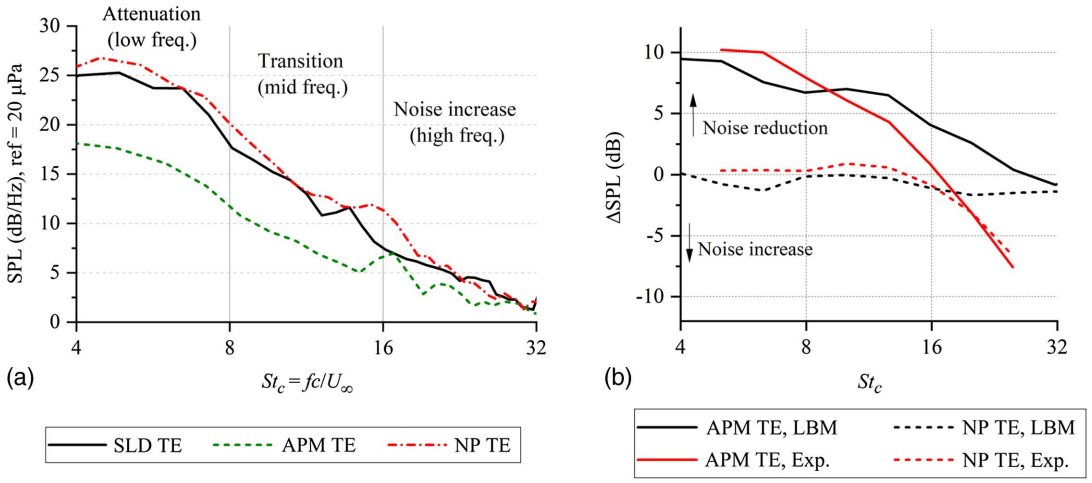

Fig. 9. (a) Comparison of far-field noise spectra among the different TE types; and (b) noise-reduction level of the APM and NP TE relative to SLD TE. Experimental results are abbreviated as Exp.

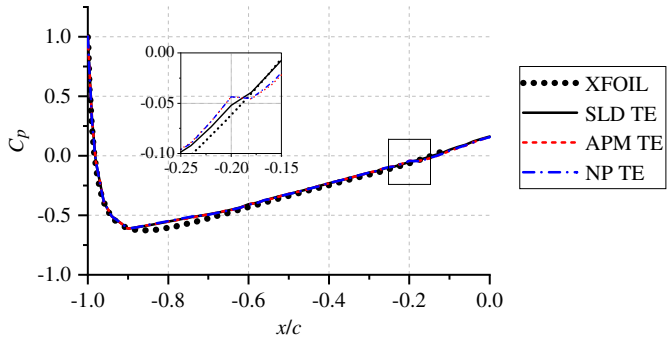

Fig. 10. Mean surface pressure distribution on the NACA 0018 with solid and porous trailing-edge configuration. The values near the tripping device ($x/c = -0.8$) are replaced with interpolated ones. The insets show the regions marked with the solid rectangles. XFOIL data were taken from Rubio Carpio et al. (2017).

The metal foam TE impact on the airfoil drag has been reported more recently (Teruna et al. 2020). The fully permeable TE was found to increase drag by almost 11% compared with its solid counterpart. Interestingly, the drag increase caused by the partially blocked porous TE is smaller at 6%, which suggests that the drag increase is influenced by the TE permeability, in agreement with other findings in the literature (Sarradj and Geyer 2007; Geyer and Sarradj 2014).

Jet Installation Noise

For jet installation noise reduction, the porous medium model is applied in the trailing-edge region of a surface in the vicinity of a subsonic jet at ambient temperature. The jet is generated by a single-stream nozzle (SMC000), with an exit diameter $D_j = 50.8$ mm, and the installation effects are accounted by positioning a flat plate of length $L = 6D_j$ and height $h = 1.5D_j$ (Rego et al. 2020) (Fig. 11). The length is defined as the distance between the nozzle

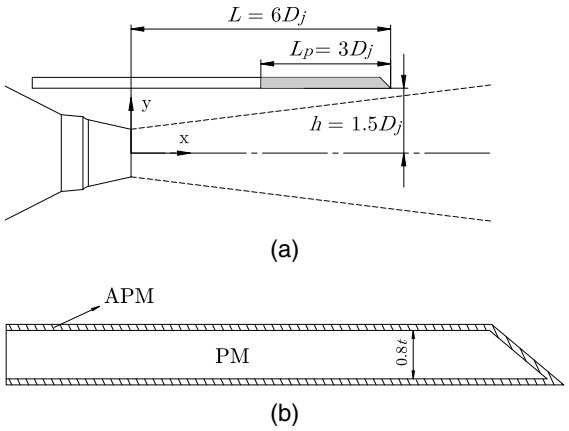

Fig. 11. (a) Installed jet setup, comprised of a single stream nozzle and a flat plate with length $L = 6D_j$ and height $h = 1.5D_j$, where the porous region of the plate has a length $L_p = 3D_j$ upstream of the trailing edge; and (b) porous medium model comprised by PM and APM regions, with the latter represented by 80% of the plate thickness t.

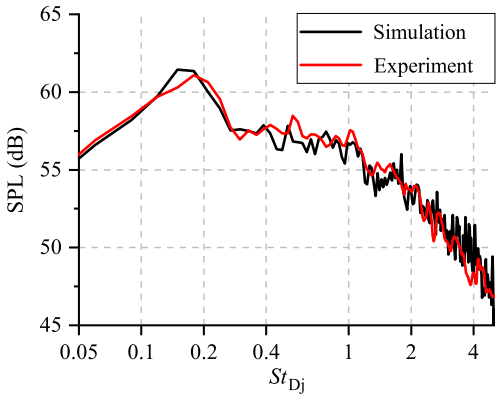

Fig. 12. SPL spectra of an installed jet with a porous trailing edge obtained from numerical simulations compared with experimental results (Rego et al. 2021). Spectra obtained for $M_a = 0.5$ jet and an observer at a position $\theta = 90°$.

exit plane and the plate trailing edge, whereas the height is defined with respect to the jet centerline, as shown in Fig. 12(b).

The porous medium model is applied on the surface with a length $L_p = 3D_j$, upstream of the trailing edge, and with the same thickness as the original solid plate ($t = 10$ mm). Similarly as performed for the previous applications, the equivalent fluid region consists of thePM-APM combination. The APM is defined with 10% of the plate thickness on both upper and lower sides, and the remaining region is set with the PM condition, as shown in Fig. 12(b). For both regions, the inertial and viscous resistivities are set based on their respective thickness, as reported in Table 1. The resistivity is the same in all three directions.

In order to verify the validity of the model for a jet installation noise application, the results from the numerical simulations are compared with experimental data by Rego et al. (2021) in terms of SPL spectra versus Strouhal number ($St = f \times D_j/U_j$). The data are obtained for a fine-resolution computational grid (Rego et al. 2020). The spectra are obtained for a jet with acoustic Mach number $M_a = 0.5$, an observer distance of $100D_j$, and polar angle $\theta = 90°$ (y-direction, normal to the jet axis) on the reflected side

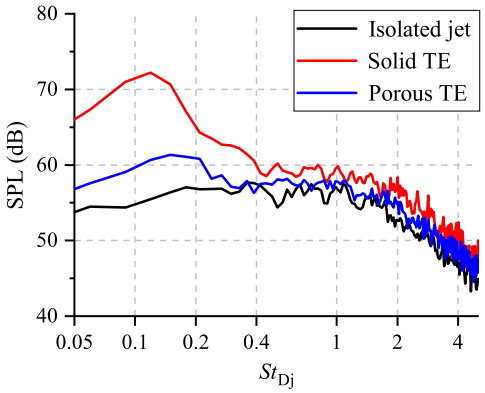

Fig. 13. SPL spectra of the installed jet with solid and porous trailing edges. The isolated jet spectrum is included as reference. Spectra obtained for $M_a = 0.5$ jet and an observer at a position $\theta = 90°$.

(negative y) of the plate for a constant-frequency band of 100 Hz. The frequency band of the experimental data has been changed to 100 Hz for a proper comparison with the computational results. A good agreement is obtained between the curves, with a maximum deviation of 1.5 dB between them. Therefore, the porous medium model of the metal foam, along with the prescribed resistivity inputs, is also applicable for a jet installation noise case.

In Fig. 13, the spectrum for the installed jet with a porous trailing edge is also compared with that of a numerical simulation of the baseline solid case in order to quantify the noise reduction provided by this solution. Spectra are again obtained for $M_a = 0.5$ and $\theta = 90°$. The isolated jet spectrum, obtained from a simulation of the nozzle without the plate, is also included as a reference. The isolated and installed (with solid TE) jet computational setups have already been validated through comparisons with experimental data (Rego et al. 2020). The results, obtained from a medium-resolution grid (Rego et al. 2020), show a significant noise reduction with respect to the reference solid case, particularly for $St < 0.4$, where installation effects are dominant. At the peak of the solid TE curve ($St = 0.12$), a reduction of 12 dB is obtained with the porous case. Therefore, it is concluded that the trailing-edge source becomes less dominant with respect to the noise produced by turbulence mixing in the jet. This is due to a better pressure balance between the upper and lower sides of the plate, thus reducing the noise due to scattering. Moreover, for $St > 0.4$, the porous TE also reduces noise due to reflection of acoustic waves on the surface.

Conclusions

An approach to simulate porous material using an equivalent fluid model based on the Darcy's law has been proposed. It is based on a three-layer approach to account for the dependence of the porous material properties with sample thickness, which separates the bulk effect from the entrance effect; the latter becomes increasingly relevant for porous material of small thicknesses. The three-layer approach has been shown to accurately reproduce the pressure-drop test rig that is used to characterize porous materials. Subsequently, this paper has provided a brief review of different applications of the porous medium models. In particular, the properties of a metal foam have been considered in simulations that address turbulence-impingement noise, turbulent boundary-layer trailing-edge noise, and jet installation noise. In all three cases, metal foam applications have been shown to possess promising noise-reduction capability.

Nevertheless, discrepancies between simulation results and those of experiments are still present in the high-frequency range due to the neglected surface roughness effects, although the general acoustic trends are still captured. In addition, further study on the applicability of the porous medium models for other types of materials is warranted to identify the limitations of the current approach. It would also be interesting to consider thin permeable materials (e.g., kevlar sheets) which are fully dominated by the entrance effect.

Data Availability Statement

Some or all data, models, or code that support the findings of this study are available from the corresponding author upon reasonable request.

Acknowledgments

This study is supported by the following projects: SMARTANSWER (Smart Mitigation of Flow-Induced Acoustic Radiation and Transmission for Reduced Aircraft, Surface Transport, Workplaces and Wind Energy Noise), which has received funding from the European Union's Horizon 2020 research and innovation program under the Marie Skłodowska-Curie Grant Agreement No. 722401. More information can be found on https://www.h2020-smartanswer.eu/; and NWO-IPERMAN Innovative Permeable Materials for Noise Reduction, Open Technology Program with Grant No. 15452 of the NWO Dutch Foundation of Research.

References

Ali, S. A. S., M. Azarpeyvand, and C. R. I. da Silva. 2018. "Trailing-edge flow and noise control using porous treatments." *J. Fluid Mech.* 850 (Sep): 83–119. https://doi.org/10.1017/jfm.2018.430.

Amiet, R. K. 1975. "Acoustic radiation from an airfoil in a turbulent stream." *J. Sound Vib.* 41 (4): 407–420. https://doi.org/10.1016/S0022-460X(75)80105-2.

Amiet, R. K. 1976. "Noise due to turbulent flow past a trailing edge." *J. Sound Vib.* 47 (3): 387–393. https://doi.org/10.1016/0022-460X(76)90948-2.

Ananthan, V., P. Bernicke, R. Akkermans, T. Hu, and P. Liu. 2020. "Effect of porous material on trailing edge sound sources of a lifting airfoil by zonal overset-LES." *J. Sound Vib.* 480 (Aug): 115386. https://doi.org/10.1016/j.jsv.2020.115386.

Baril, E., A. Mostafid, L.-P. Lefebvre, and M. Medraj. 2008. "Experimental demonstration of entrance/exit effects on the permeability measurements of porous materials." *Adv. Eng. Mater.* 10 (9): 889–894. https://doi.org/10.1002/adem.200800142.

Brès, G., F. Pérot, and D. Freed. 2010. "A Ffowcs Williams - Hawkings solver for lattice-Boltzmann based computational aeroacoustics." In *Proc., 16th AIAA/CEAS Aeroacoustics Conf.* Reston, VA: American Institute of Aeronautics and Astronautics.

Brooks, T. F., and W. M. Humphreys Jr. 2003. "Flap-edge aeroacoustic measurements and predictions." *J. Sound Vib.* 261 (1): 31–74. https://doi.org/10.1016/S0022-460X(02)00939-2.

Casalino, D. 2003. "An advanced time approach for acoustic analogy predictions." *J. Sound Vib.* 261 (4): 583–612. https://doi.org/10.1016/S0022-460X(02)00986-0.

Casalino, D., A. Hazir, and A. Mann. 2018. "Turbofan broadband noise prediction using the lattice Boltzmann method." *AIAA J.* 56 (2): 609–628. https://doi.org/10.2514/1.J055674.

Cavalieri, A., W. Wolf, and J. Jaworski. 2016. "Numerical solution of acoustic scattering by finite perforated elastic plates." *Proc. R. Soc. A: Math. Phys. Eng. Sci.* 472 (2188): 20150767. https://doi.org/10.1098/rspa.2015.0767.

Chanaud, R., N. Kong, and R. Sitterding. 1976. "Experiments on porous blades as a means of reducing fan noise." *J. Acoust. Soc. Am.* 59 (3): 564–575. https://doi.org/10.1121/1.380900.

Chen, H., S. Chen, and W. H. Matthaeus. 1992. "Recovery of the Navier-Stokes equations using a lattice-gas Boltzmann method." *Phys. Rev. A* 45 (8): R5339. https://doi.org/10.1103/PhysRevA.45.R5339.

Chen, H., S. A. Orszag, I. Staroselsky, and S. Succi. 2004. "Expanded analogy between Boltzmann kinetic theory of fluids and turbulence." *J. Fluid Mech.* 519 (Nov): 301–314. https://doi.org/10.1017/S0022112004001211.

Delfs, J., B. Faßmann, N. Lippitz, M. Lummer, M. Mößner, L. Müller, K. Rurkowska, and S. Uphoff. 2014. "SFB 880: Aeroacoustic research for low noise take-off and landing." *CEAS Aeronaut. J.* 5 (4): 403–417. https://doi.org/10.1007/s13272-014-0115-2.

Farassat, F., and G. P. Succi. 1980. "A review of propeller discrete frequency noise prediction technology with emphasis on two current methods for time domain calculations." *J. Sound Vib.* 71 (3): 399–419. https://doi.org/10.1016/0022-460X(80)90422-8.

Ffowcs-Williams, J. E., and D. L. Hawkings. 1969. "Sound generation by turbulence and surfaces in arbitrary motion." *Philos. Trans. R. Soc. A: Math. Phys. Eng. Sci.* 264 (1151): 321–342.

Freed, D. M. 1998. "Lattice-Boltzmann method for macroscopic porous media modeling." *Int. J. Mod. Phys. C* 9 (08): 1491–1503. https://doi.org/10.1142/S0129183198001357.

Geyer, T. F., and E. Sarradj. 2014. "Trailing edge noise of partially porous airfoils." In *Proc., 20th AIAA/CEAS Aeroacoustics Conf.*, 3039. Reston, VA: American Institute of Aeronautics and Astronautics.

Geyer, T. F., and E. Sarradj. 2019. "Self noise reduction and aerodynamics of airfoils with porous trailing edges." *Acoustics* 1 (2): 393–409. https://doi.org/10.3390/acoustics1020022.

Hayden, R. E. 1973. "Fundamental aspects of noise reduction from powered-lift devices." *SAE Trans.* 82: 1287–1306.

Herr, M., and W. Dobrzynski. 2005. "Experimental investigations in low-noise trailing edge design." *AIAA J.* 43 (6): 1167–1175. https://doi.org/10.2514/1.11101.

Herr, M., K.-S. Rossignol, J. Delfs, N. Lippitz, and M. Mößner. 2014. "Specification of porous materials for low-noise trailing-edge applications." In *Proc., 20th AIAA/CEAS Aeroacoustics Con.*, 3041. Reston, VA: American Institute of Aeronautics and Astronautics.

Howe, M. S. 1978. "A review of the theory of trailing edge noise." *J. Sound Vib.* 61 (3): 437–465. https://doi.org/10.1016/0022-460X(78)90391-7.

Ingham, D. B., and I. Pop. 1998. *Transport phenomena in porous media.* Amsterdam, Netherlands: Elsevier.

Jacob, M. C., J. Boudet, D. Casalino, and M. Michard. 2005. "A rod-airfoil experiment as a benchmark for broadband noise modeling." *Theor. Comput. Fluid Dyn.* 19 (3): 171–196. https://doi.org/10.1007/s00162-004-0108-6.

Jiang, C., Y. Yauwenas, J. Fischer, D. Moreau, C. Doolan, J. Gao, W. Jiang, R. McKay, and M. Kingan. 2018. "Control of rotor trailing edge noise using porous additively manufactured blades." In *Proc., 2018 AIAA/CEAS Aeroacoustics Conf.* Reston, VA: American Institute of Aeronautics and Astronautics..

Kisil, A., and L. J. Ayton. 2018. "Aerodynamic noise from rigid trailing edges with finite porous extensions." *J. Fluid Mech.* 836 (Feb): 117–144. https://doi.org/10.1017/jfm.2017.782.

Kshetrimayum, R. S. 2004. "A brief intro to metamaterials." *IEEE Potentials* 23 (5): 44–46. https://doi.org/10.1109/MP.2005.1368916.

Kuwata, Y., and K. Suga. 2017. "Direct numerical simulation of turbulence over anisotropic porous media." *J. Fluid Mech.* 831 (Nov): 41–71. https://doi.org/10.1017/jfm.2017.619.

Launder, B. E., and D. B. Spalding. 1974. "The numerical computation of turbulent flows." *Comput. Methods Appl. Mech. Eng.* 3 (2): 269–289. https://doi.org/10.1016/0045-7825(74)90029-2.

Lawrence, J. L. T., M. Azarpeyvand, and R. H. Self. 2011. "Interaction between a flat plate and a circular subsonic jet." In *Proc., 17th AIAA/CEAS Aeroacoustics Conf.* Reston, VA: American Institute of Aeronautics and Astronautics.

Lee, D.-J., and C. Smith. 1991. "Effect of vortex core distortion on blade-vortex interaction." *AIAA J.* 29 (9): 1355–1362. https://doi.org/10.2514/3.10746.

Li, X., X. Li, and C. Tam. 2011. "Construction and validation of a broadband time domain impedance boundary condition." In *Proc., 17th AIAA/CEAS Aeroacoustics Conf. (32nd AIAA Aeroacoustics Conf.)*, 2870. Reston, VA: American Institute of Aeronautics and Astronautics.

Liu, H., M. Azarpeyvand, J. Wei, and Z. Qu. 2015. "Tandem cylinder aerodynamic sound control using porous coating." *J. Sound Vib.* 334 (Jan): 190–201. https://doi.org/10.1016/j.jsv.2014.09.013.

Merino-Martínez, R., A. R. Carpio, L. T. L. Pereira, S. van Herk, F. Avallone, D. Ragni, and M. Kotsonis. 2020. "Aeroacoustic design and characterization of the 3D-printed, open-jet, anechoic wind tunnel of Delft University of Technology." *Appl. Acoust.* 170 (Dec): 107504. https://doi.org/10.1016/j.apacoust.2020.107504.

Morreale, B., and F. Shi. 2015. *Novel materials for carbon dioxide mitigation technology.* Amsterdam, Netherlands: Elsevier.

Narayanan, S., P. Chaitanya, S. Haeri, P. Joseph, J. Kim, and C. Polacsek. 2015. "Airfoil noise reductions through leading edge serrations." *Phys. Fluids (1994)* 27 (2): 025109. https://doi.org/10.1063/1.4907798.

Oerlemans, S., M. Fisher, T. Maeder, and K. Kögler. 2009. "Reduction of wind turbine noise using optimized airfoils and trailing-edge serrations." *AIAA J.* 47 (6): 1470–1481. https://doi.org/10.2514/1.38888.

Rego, L., F. Avallone, D. Ragni, and D. Casalino. 2020. "Jet-installation noise and near-field characteristics of jet-surface interaction." *J. Fluid Mech.* 895 (A2): 1–37. https://doi.org/10.1017/jfm.2020.294.

Rego, L., D. Ragni, F. Avallone, D. Casalino, R. Zamponi, and C. Schram. 2021. "Jet-installation noise reduction with flow-permeable materials." *J. Sound Vib.* 498: 115959. https://doi.org/10.1016/j.jsv.2021.115959.

Roger, M., C. Schram, and L. De Santana. 2013. "Reduction of airfoil turbulence-impingement noise by means of leading-edge serrations and/or porous material." In *Proc., 19th AIAA/CEAS Aeroacoustics Conf.*, 2108. Reston, VA: American Institute of Aeronautics and Astronautics.

Rouquerol, J., D. Avnir, C. Fairbridge, D. Everett, J. Haynes, N. Pernicone, J. Ramsay, K. Sing, and K. Unger. 1994. "Recommendations for the characterization of porous solids (technical report)." *Pure Appl. Chem.* 66 (8): 1739. https://doi.org/10.1351/pac199466081739.

Rubio Carpio, A., F. Avallone, and D. Ragni. 2018. "On the role of the flow permeability of metal foams on trailing edge noise reduction." In *Proc., 2018 AIAA/CEAS Aeroacoustics Conf.*, 2964. Reston, VA: American Institute of Aeronautics and Astronautics.

Rubio Carpio, A., F. Avallone, D. Ragni, M. Snellen, and S. van der Zwaag. 2019. "Mechanisms of broadband noise generation on metal foam edges." *Phys. Fluids (1994)* 31 (10): 105110. https://doi.org/10.1063/1.5121248.

Rubio Carpio, A., F. Avallone, D. Ragni, M. Snellen, and S. van der Zwaag. 2020. "Quantitative criteria to design optimal permeable trailing edges for noise abatement." *J. Sound Vib.* 485: 115596. https://doi.org/10.1016/j.jsv.2020.115596.

Rubio Carpio, A., R. Merino Martinez, F. Avallone, D. Ragni, M. Snellen, and S. van der Zwaag. 2017. "Broadband trailing-edge noise reduction using permeable metal foams." In Vol. 255 of *Proc., INTER-NOISE and NOISE-CON Congress and Conf.*, 2755–2765. Hongkong, China: Institute of Noise Control Engineering.

Sarradj, E., and T. Geyer. 2007. "Noise generation by porous airfoils." In *Proc., 13th AIAA/CEAS Aeroacoustics Conf. (28th AIAA Aeroacoustics Conf.)*, 3719. Reston, VA: American Institute of Aeronautics and Astronautics.

Self, R. 2004. "Jet noise prediction using the Lighthill acoustic analogy." *J. Sound Vib.* 275 (3–5): 757–768. https://doi.org/10.1016/j.jsv.2003.06.020.

Succi, S. 2001. *The lattice Boltzmann equation for fluid dynamics and beyond*. Oxford, UK: Oxford University Press.

Sun, C., F. Pérot, R. Zhang, P.-T. Lew, A. Mann, V. Gupta, D. M. Freed, I. Staroselsky, and H. Chen. 2015. "Lattice Boltzmann formulation for flows with acoustic porous media." *Comptes Rendus Mécanique* 343 (10–11): 533–544. https://doi.org/10.1016/j.crme.2015.07.013.

Teruna, C., F. Avallone, D. Casalino, and D. Ragni. 2021. "Numerical investigation of leading edge noise reduction on a rod-airfoil configuration using porous materials and serrations." *J. Sound Vib.* 494 (Mar): 115880. https://doi.org/10.1016/j.jsv.2020.115880.

Teruna, C., F. Manegar, F. Avallone, D. Ragni, D. Casalino, and T. Carolus. 2020. "Noise reduction mechanisms of an open-cell metal-foam trailing edge." *J. Fluid Mech.* 898 (A18): 1–36. https://doi.org/10.1017/jfm.2020.363.

Wie, S.-Y., D.-K. Im, J.-H. Kwon, D.-J. Lee, K. Chung, and S. Kim. 2011. "Helicopter rotor noise in the merged tip-vortex and blade interaction condition." *Int. J. Aeroacoust.* 10 (4): 427–442. https://doi.org/10.1260/1475-472X.10.4.427.

Yakhot, V., and S. A. Orszag. 1986. "Renormalization group analysis of turbulence. I. Basic theory." *J. Sci. Comput.* 1 (1): 3–51. https://doi.org/10.1007/BF01061452.

Zamponi, R., S. Satcunanathan, S. Moreau, D. Ragni, M. Meinke, W. Schröder, and C. Schram. 2020. "On the role of turbulence distortion on leading-edge noise reduction by means of porosity." *J. Sound Vib.* 485 (Oct): 115561. https://doi.org/10.1016/j.jsv.2020.115561.